Cent. Eur. J. Geosci. • 1(4) • 2009 • 443-455
DOI: 10.2478/v10085-009-0031-6

VERSITA

Central European Journal of **Geosciences**

# Surface wind speed probability distribution in the Southeast Pacific of Marine Stratus and Stratocumulus regions

**Research Article**

Yanping He*

*School of Earth and Ocean Science, University of Victoria, Victoria, BC, V8W3P6, Canada*

**Received 18 May 2009; accepted 20 September 2009**

**Abstract:** Probability distributions of surface wind speeds (SWS) near coastal regions are needed for applications such as estimating offshore wind power and ocean surface fluxes and for offshore wind risk assessments. Ocean surface wind speed probability distribution (PDF) is characterized using three-year QuikSCAT and AIRS satellite observations in the southeast Pacific of marine stratus and stratocumulus (MSC) regions. Seasonal variation is removed from wind statistics. It was found that the observed SWS standard deviation has a linear positive relationship with its mean SWS; while the SWS skewness decreases with mean SWS in regimes of strong winds and increases with mean SWS in regimes of weak winds. A simple 1D conceptual model is developed near the Peruvian region, which successfully reproduces the observed relationship between higher moments of SWS and its mean value. The model based physical picture among ocean surface winds, SST, and marine boundary clouds are supported by three-year QuikSCAT surface wind observations and fifteen-year ERA40 re-analysis data. Model sensitive tests suggest that large-scale divergence, and strengths of momentum and cloud fluctuations have significant effects on the ocean SWS-PDF in marine stratus and stratocumulus regions.

**Keywords:** probability distribution of ocean surface wind speed • marine stratus and stratocumulus • large-scale subsidence • SST



## 1. Introduction

Knowledge of ocean surface wind speed (SWS) probability distribution function (PDF) has important applications in offshore wind energy development and management, extreme wind assessment, and surface flux parameterizations [1–4]. A number of studies have examined the parameterization of wind PDFs using surface wind speed [4–7, 9–11]. However, no previous work has addressed how interactions of ocean surface SST, large-scale divergence, and marine boundary clouds affect ocean SWS-PDF.

In offshore regions, extensive marine stratus and stratocumulus (MSC) covers a large fraction of the ocean surface. It has a complicated spatial structure and rich internal variability, which combines the factors of slowly varying planetary scale processes with randomly fluctuating turbulence. Various studies have linked SST and large-scale circulation to the mean ocean SWS and MSC. Influences of SST on boundary layer winds have been investigated in previous studies [12]. A diagnostic study of Nigam et al. [8]

*E-mail: yhe@uvic.ca

suggested a positive feedback between surface winds, marine boundary clouds, and surface flux in the southeast Pacific regions. Recent work of He [13] also provided various lines of evidence to demonstrate that both large-scale circulations and local thermal structures control the seasonal and interannual variations of boundary layer cloudiness in subtropical MSC regions. In the southeast Pacific, ocean SWS are also strongly influenced by mixing layer depth variations due to in-cloud radiation heterogeneity, cloud-top entrainment variations, and move in and out of tropics wave and middle latitude synoptic systems. As a natural consequence, ocean SWS-PDF in offshore regions such as in the southeast Pacific is a result of multi-scale interactions among clouds, ocean, and atmosphere.

Satellite observations have revolutionized our ability to gather high resolution ocean surface winds and cloud cover information globally. The SeaWinds instrument abroad the Quik Scatterometer (QSCAT) satellite was launched in 1999 and has generated daily ocean surface winds at 0.25°×0.25° resolution since its launch. The Atmospheric InfraRed Sounder (AIRS) satellite was launched in 2002 and has generated cloud cover, cloud liquid water path, and 3-D temperature profiles at a 1°×1° horizontal resolution over three years. These high-resolution continuous satellite datasets provide remarkable opportunities to study ocean SWS-PDF in marine low clouds regions, which have been used to explore global wind climatology [14, 15].

The objective of this study is to characterize and simulate ocean SWS-PDF in marine low cloud regions, combining satellite observations with a conceptual stochastic model. The datasets used are described and observational results are documented. A highly simplified 1D deterministic model is developed to explain the QUIKSCAT and ERA40 observed mean state relationship. Stochastic perturbations are added into this conceptual model, which simulates well the observed relationship between higher moments of SWS and its mean value. The influences of various factors on ocean SWS-PDF are also discussed..

## 2. Data descriptions

QuikSCAT sea surface wind dataset consists of Level 2.0 and Level 3.0 gridded daily SeaWinds scatterometer 10 m zonal and meridional wind observations from the NASA QuikSCAT satellite (Jet Propulsion Laboratory, 2001), available on a 0.25°×0.25° grid from March, 2003 to February, 2006. The level 3 gridded data is used in this study, which is first averaged into 1°×1° grid resolution for the same time period. Because rainfall can lead to errors in estimating sea surface winds, the data points with rainfall flags in Level 3 are excluded from the present analysis. The cloud cover dataset consists of the Level 3.0 Gridded Retrieval Product from the NASA AIRS satellite (http://disc.gsfc.nasa.gov/AIRS), available on an 1°×1° horizontal resolution from March 2003 to February 2006, the same period as that of the QUIKSCAT surface wind dataset. The study period of QuikSCAT and AIRS satellite data in this paper is from March 2003 to February 2006 in the southeast Pacific (100W - 80W, 30S - 10S).

The ISCCP D-series dataset is also used, which provides three-hour cloud cover information at a 2.5°×2.5° horizontal resolution [16]. Its low cloud cover is the sum of cloud amounts in all low cloud types.

The ERA-40 six-hour surface wind, boundary layer height, and surface pressure at 1000 hPa used in this study are obtained from the ERA-40 website at http://data-portal.ecmwf.int/data/d/era40%5Fdaily/ [17].

## 3. Observational results

### 3.1. Observed relationship between mean winds and marine low clouds

To understand ocean surface wind probability distribution in MSC regions, it is important to understand the basic relationship between mean states of ocean surface winds with marine low clouds in the southeast Pacific. In the subsiding branch of the tropical large scale circulation, strong large scale subsidence and cold ocean surface SST lead to a large amount of dry static energy which is transported from the free atmosphere into the boundary layer. More marine low clouds are developed to adjust the local thermal structure toward a preferred mean state, such that the lower troposphere available potential temperature is well kept. When the marine cloud fraction is increased, strong cloud top radiative cooling deepens the cloud-topped boundary layer and enhances ocean surface pressure gradients. As a result, the surface southerly winds become stronger. The increased surface wind speed further deepens the mixing layer depth through larger surface flux and increases the horizontal transport of lower tropospheric dry static energy, resulting in even more marine low clouds.

This relationship between surface winds, low-level clouds, ocean SST, and large-scale subsidence is supported by previous simple model studies [18] and a diagnostic climate modeling study [8]. The suggested relationship between mean surface winds and low cloud fractions are supported by satellite observations shown in Figure 1 and by ERA-40 reanalysis products shown in Figure 2 near the Peruvian region. Figure 1 shows three-year mean

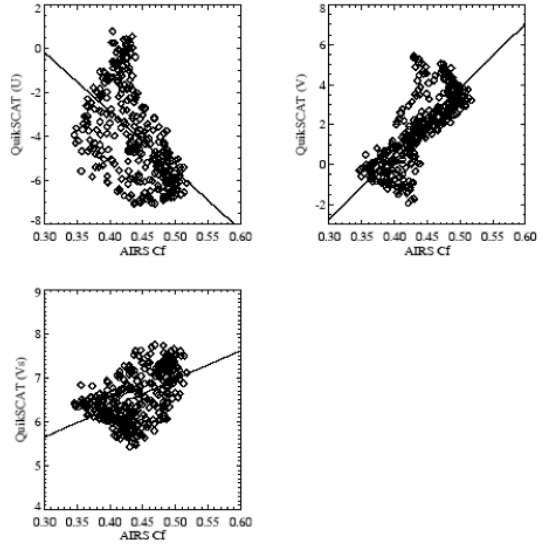


**Figure 1.** Three-year averaged QUIKSCAT surface wind speed plotted against mean AIRS cloud cover using 1°×1° grid value in the southeast Pacific (30S - 10S, 100W - 80W). The three-year mean value is averaged from March 2003 to February 2006.

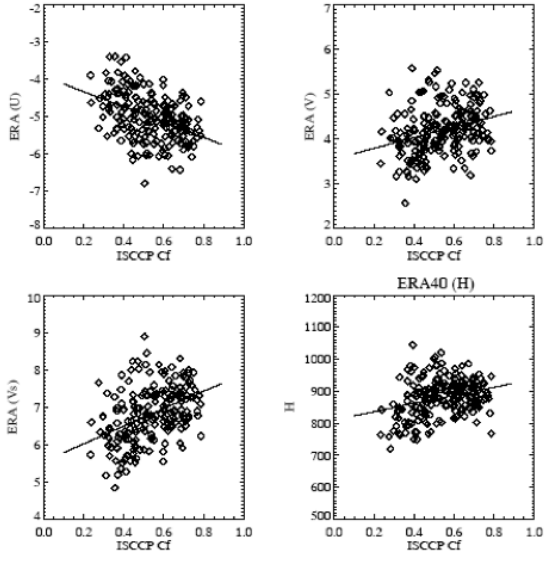


**Figure 2.** Area-averaged (a) ERA40 monthly mean zonal wind (upper left), (b) ERA40 monthly mean meridional wind (upper right), (c) ERA40 monthly mean surface wind speed (lower left), and (d) ERA40 monthly mean boundary layer height (lower right) plotted against ISCCP D-series monthly mean low cloud amount near the Peruvian region during the period of 1985 to 2000.

values of QuikSCAT surface wind speed plotted against mean AIRS cloud cover for each 1°×1° region in the south east Pacific (25S - 10S, 100W - 80W). The three-year mean value is averaged from March 2003 to February 2006. Cloud fraction increase is related to a three-year mean surface southerly wind increase. The surface wind speed is moderately increased with cloud fraction in the southeast Pacific. Figure 2 also shows the observed positive relationships of area-averaged monthly mean ERA40 ocean surface wind and boundary layer height, with area-averaged ISCCP D-series monthly low cloud fraction near the Peruvian region, during the period of 1985 to 2000.

## 3.2. Observed relationship between high moments and its mean value of non-seasonal SWS

Ocean surface winds include both mean and fluctuation components. The later is composed by seasonal variations and non-seasonal variations such as synoptic activity and eddy fluctuations. The seasonal variations of ocean surface wind and marine boundary clouds are determined primarily by the seasonal marching of solar heating and underlying ocean surface properties. However, the non-seasonal variations of ocean surface wind and boundary clouds have rich internal and random fluctuations in both spatial and temporal dimensions [19]. To characterize and understand non-seasonal SWS-PDF is important to improve surface flux estimation, offshore wind power forecast, and extreme wind risk assessment in MSC regions.

The standard deviation (upper panel) and the skewness (lower panel) of SWS are plotted against its mean value of QuikSCAT non-seasonal SWS for a three-year period in Figure 3a and for each season period in Figure 3b. Seasonal cycles are removed from the original QuikSCAT level 3 data. A positive relationship between the standard deviation and its mean value is evident in Figure 3. A negative relationship between the skewness and its mean value is found in regimes of large winds, which is consistent with previous theoretical study of ocean SWS-PDF under neutral ocean surface [9]; while in buoyancy controlled small winds regimes, the observed skewness is found to increase with increasing surface wind speed.

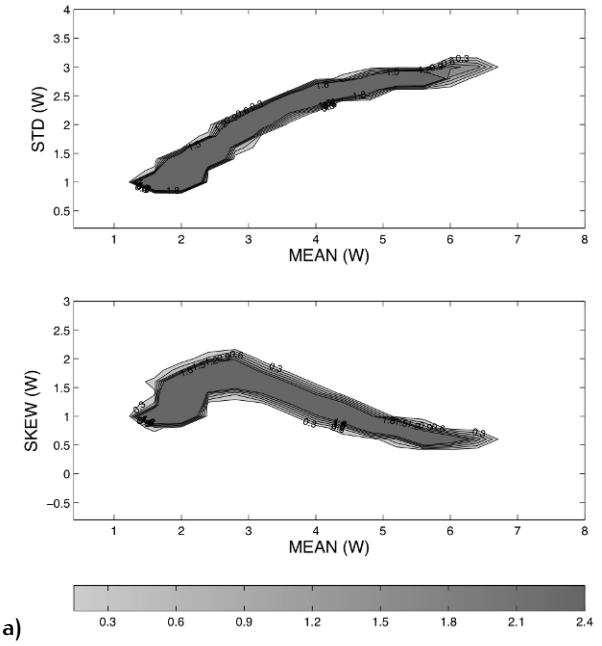


a)

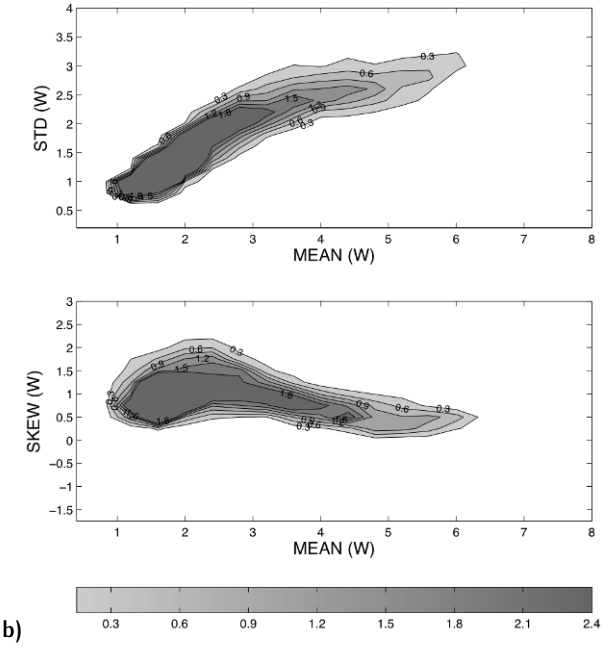


b)

**Figure 3.** The QuikSCAT mean value (upper panel), the standard deviation (middle panel), and the skewness (lower panel) are plotted against the QuikSCAT mean SWS for a three-year period in Figure 3a, and for every season period in Figure 3b, in the southeast Pacific (30S - 10S, 100W - 80W) during the period from March 2003 to February 2006. The seasonal variations have been removed from the original data.

# 4. A simple deterministic model for mean states of ocean surface winds

In the southeast Pacific, both ocean surface SST and marine boundary layer height have large horizontal gradients, which determine the ocean surface pressure gradients in MSC regions. When SST is cold, stronger dynamical transport of lower tropospheric dry static energy and larger surface evaporation enhance cloud top entrainment, deepen the marine boundary layer, increase the low cloud amount, and strengthen surface wind speeds. A simple deterministic model is developed as a foundation for ocean SWS-PDF simulation.

## 4.1. Model development

The eddy-averaged horizontal momentum equations and Lilly's simple mixing layer model [20] is combined to represent the ocean surface wind and marine boundary layer.

$$\partial_t U - fV = -\rho^{-1}\partial_x P_s - \partial_z\left(\overline{w'u'}\right), \quad (1)$$

$$\partial_t V + fU = -\rho^{-1}\partial_y P_s - \partial_z\left(\overline{w'v'}\right), \quad (2)$$

$$\partial_t h = w_e - D_{zi}h. \quad (3)$$

In Equations (1) to (3), $U$represents the near surface zonal wind, $V$ represents the near surface meridional wind, $\overline{w'u'}$ and $\overline{w'v'}$ are surface wind stress for zonal wind and meridional wind, $D_{zi}$ represents divergence at the boundary layer top, $f$ is the Coriolis parameter, $h$ is the boundary layer height, $w_e$ is the entrainment rate, $\rho$ is the air density, $P_s$ is the surface air pressure. Some other variables used in this paper are also listed here; $\theta$ is the boundary layer potential temperature, $q$ is the boundary layer specific humidity, $q_s$ is the saturated specific humidity, $T_s$ is the ocean surface temperature, $C_h$ and $C_e$ are surface heat and moisture transfer coefficient respectively, $P$ is precipitation, $\beta$ is local efficient of precipitation. Horizontal and vertical advection terms are not considered in the model.

### 4.1.1. Near surface pressure perturbations

The lower troposphere is characterized by a two-layer structure shown in Figure 4, with a cold moist boundary layer topped by a warm and dry free atmosphere below the trade wind inversion at $Z_T$. The boundary layer cloud occurs near the boundary layer top beneath a strong temperature inversion. The air density in the boundary layer is $\rho_{Bl}$ and the air density in the free atmosphere is $\rho_{free}$. The surface pressure $P_s$ is determined by the air pressure at the trade wind inversion $P_T$ and the air density in the lower troposphere.

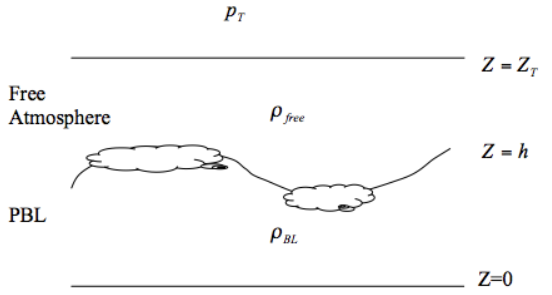


**Figure 4.** A carton of a two-layered structure within the lower troposphere.

$$P_s = P_T + \int_0^{Z_T} \rho g dz = P_T + g\int_0^h \rho_{BL} dz + g\int_h^{Z_T} \rho_{free} dz. \quad (4)$$

Here $\rho_{BL}$ and $\rho_{free}$ represent air density within boundary layer and free atmosphere respectively, and $P_T$ is air pressure at trade wind inversion. The air density perturbation is proportional to potential temperature perturbation. The surface air pressure can be formulated as function of boundary layer height and potential temperature difference between free atmosphere and ocean surface.

$$P_S = P_T + g\tilde{\rho}_{free} Z_T + g\rho_0 \frac{\Delta\theta}{\theta_0} h. \quad (5)$$

Here $\Delta\theta = \tilde{\theta}_{free} - \tilde{\theta}_{BL} \approx \theta_{Z_t} - \theta_{srf}$ is the potential temperature difference between trade wind inversion and the ocean surface. The pressure and height gradients at the trade wind inversion are assumed to vanish; therefore the surface pressure gradient is determined by both the boundary layer height variation and lower troposphere stability gradient.

$$\nabla P_s \approx g\frac{\overline{\Delta\theta}}{\theta_0}\nabla h + \frac{gh}{\theta_2}\nabla(\Delta\theta). \quad (6)$$

In a highly simplified case, it is assumed that the amplitude of horizontal gradient of the boundary layer height is proportional to the boundary layer height. From ERA40 re-analysis (not shown here), $\Delta\theta$ increases towards the coastal region, and decreases from the south towards the equator due to the distribution of SSTs. The boundary layer height decreases towards the coastal region and towards the equator. The west-east gradient of $\Delta\theta$ weakens $\nabla_x P_s$; while the boundary layer height variation enhances $\nabla_x P_s$ and dominates the west-east surface pressure termination. South-north gradients of both $\Delta\theta$ and boundary layer height contribute to negative $\nabla_y P_s$. Based on ERA40 results near the Peruvian region, in this simple model, the mean surface pressure gradient is determined primarily by the boundary layer height, and the gradient of the temperature inversion strength is given a constant value.

$$\nabla_x P_s \approx g\left(\frac{\Delta\theta}{L_x}\right)\frac{h}{\theta_0} \approx g\left(\frac{-1.35\ \mathrm{K}}{100\ \mathrm{KM}}\right)\frac{h}{\theta_0} = a_u \Delta\theta h, \quad (7)$$

$$\nabla_y P_s \approx g\left(\frac{\Delta\theta}{L_y}\right)\frac{h}{\theta_0} \approx g\left(\frac{-1.01K}{100KM}\right)\frac{h}{\theta_0} = a_v \Delta\theta h. \quad (8)$$

#### 4.1.2. Surface wind stress

Based on bulk formula, surface wind stress is parameterized by surface wind speed $V_s$ and the drag coefficient $C_d$, using the following formulas:

$$\overline{w'u'} \approx C_d V_s U, \quad (9)$$

$$\overline{w'v'} \approx C_d V_s V. \quad (10)$$

A typical value for $C_d$ is $1.18 \times 10^{-3}$ for wind speed less than 10 m/s over the tropical ocean. The vertical shear of ocean wind stress is simplified as

$$\partial_z \overline{w'x'} = C_d V_s \frac{X}{H_0}. \quad (11)$$

In Equation (11), $H_0$ is the mixing layer depth taken to be 500 m in this highly simplified study.

#### 4.1.3. Entrainment rate due to buoyancy

Following Lilly's entrainment idea [20], entrainment heating is partially balanced by cloud top radiative cooling near the inversion layer.

$$c_p \rho w_e \Delta^+\theta = \gamma C_f F^0_{crf}. \quad (12)$$

In Equation (12), $\gamma \in [0,1]$ is the ratio of cloud top radiative cooling to balance entrainment heating. From ISCCP FD observation [13], unit area cloud top radiative cooling is $F^0_{crf} = 70\ \mathrm{Wm}^{-2}$. As in Lilly's model, the temperature inversion strength near the boundary top is linearly determined by lower troposphere stability $\theta_{Z_T} - T_s$ and boundary layer height.

$$\Delta^+\theta = \left(\theta_{Z_T} - T_s\right)\frac{h}{Z_T}. \quad (13)$$

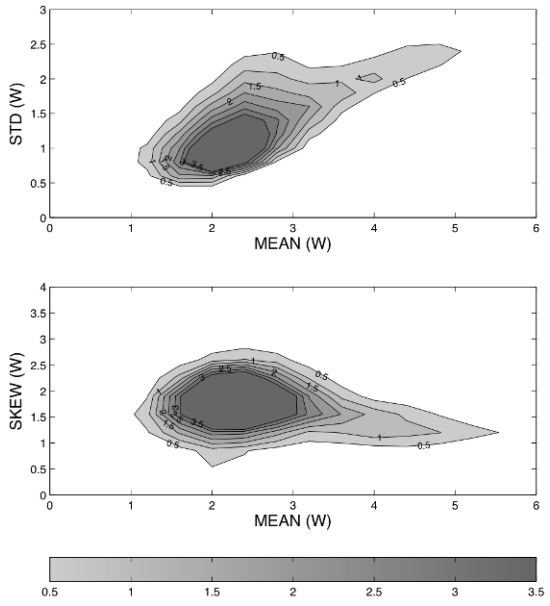


**Figure 5.** Model simulated surface wind mean value (upper panel), the standard deviation (middle panel), and the skewness (lower panel), as functions of surface mean wind speed. The seasonal variation is removed from the original surface winds.

#### 4.1.4. Boundary layer cloud amount

From He [13], cloud top radiative cooling is balanced by the dynamical transport of lower troposphere dry static energy E.

$$\varepsilon A_{dyn}(E) + \beta F_{LH} - C_f F^0_{crf} \approx 0, \tag{14}$$

$$A_{dyn}(E) = \rho c_p \left[ -W_h \left( \theta_{Z_T} - T_s \right) + \int_0^{Z_T} \left( U\partial_x + V\partial_y \right) \left( \theta_{env} - \theta_{pal} \right) dz \right]. \tag{15}$$

Surface latent heat flux $F_{LH}$ is determined by surface wind speed, ocean surface SST, and near surface relative humidity. Based on bulk formula and He [13], surface evaporation is formulated as

$$F_{LH} = L_v C_e V_s (q_s - q_a) = L_v C_e V_s \Delta q_0 \left( 1 - \frac{\Delta\theta}{\Delta\theta_{\max}} \right). \tag{16}$$

It is reasonable to set the maximum inversion strength $\Delta\theta_{\max}$ as a constant of 35 K based on the fact that the observed relationship between lower troposphere stability and near surface relative humidity as evidenced in Figure 5 is close to linear in the southeast Pacific. The empirical coefficient of humidity difference is $\Delta q_0 = 8 \times 10^{-3}$ Kg/Kg, the heat transfer coefficient is $C_e = 3 \times 10^{-3}$. From ERA40 re-analysis, large-scale divergence is relatively unchanged near the surface. Therefore, large-scale vertical velocity at the boundary layer top is a function of large-scale divergence and boundary layer height.

$$W_{Z_i} = -D_{Zi} h. \tag{17}$$

Horizontal transport of E is assumed to depend mainly on near surface winds.

$$\int_0^{Z_T} \left( U\partial_x + V\partial_y \right) \left( \theta_{env} - \theta_{pal} \right) dz \approx t_u U + t_v V, \tag{18}$$

$$\begin{aligned} t_u &= \int_0^{Z_T} \partial_x (\theta_{env} - \theta_{pal}) dz, \\ t_v &= \int_0^{Z_T} \partial_y (\theta_{env} - \theta_{pal}) dz. \end{aligned} \tag{19}$$

In the model simulations, $t_u$ and $t_v$ are given values of $2.5 \times 10^{-3}$ Km/s and $-2.5 \times 10^{-3}$ Km/s respectively based on the climatology of the southeast Pacific. Combining Equations (14)-(19), low cloud fraction $C_f$ is formulated as the function of large-scale divergence, SST, boundary layer height, and near-surface winds.

$$0.3 c_p \left[ -D_{zi} h (\theta_{700} - T_s) - t_u U - t_v V \right] + a_c V_s \Delta q \left[ 1 - \frac{\theta_{Z_T} - T_s}{\Delta\theta_{\max}} \right] = C_f F^0_{crf}, \tag{20}$$

$$a_c = \beta L_v C_e. \tag{21}$$

The 1D conceptual model after parameterizations is written as

$$\partial_t U = a_u (\theta_{Z_T} - T_s) h + fV - C_d V_s \frac{U}{h_0}, \tag{22}$$

$$\partial_t V = a_v (\theta_{Z_T} - T_s) h - fU - C_d V_s \frac{V}{h_0}, \tag{23}$$

$$\partial_t h = \frac{\gamma C_f F^0_{crf} Z_T}{h \left( \theta_{Z_T} - T_s \right)} - D_{zi} h, \tag{24}$$

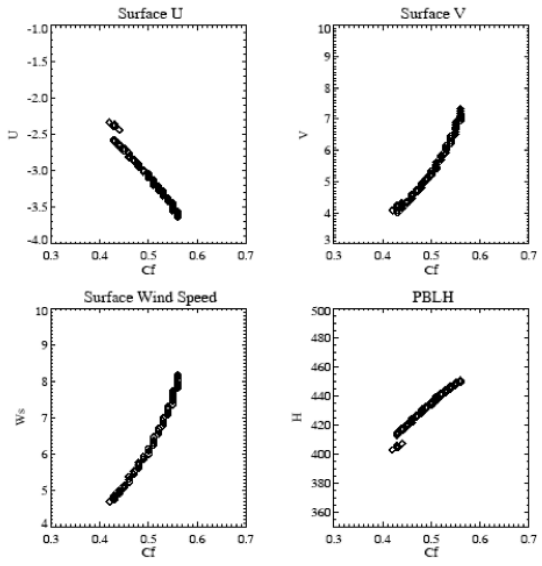


**Figure 6.** Model simulated equilibrium surface wind and boundary layer height as a function of marine cloud amount. The large-scale divergence is set to $5 \times 10^{-6}$ s$^{-1}$.

$$C_f F^0_{crf} = 0.3 c_p \left[ D_{zi} h (\theta_{Z_T} - T_s) - t_u U - t_v V \right] + a_c V_s \Delta q_0 \left[ 1 - \frac{\theta_{Z_T} - T_s}{\Delta \theta_{\max}} \right]. \quad (25)$$

Prescribed model forcing includes large-scale divergence at cloud top $D_{Z_i}$ and ocean surface SST. The potential temperature at trade wind inversion $\theta_{Z_T}$ is given a climatology value of 312 K near the Peruvian region.

## 4.2. Simulation results

In Figure 6, equilibrium solutions of surface easterly wind, southerly wind, surface wind speed, and boundary layer height are shown as functions of marine low cloud fraction. In the model simulation run, SST is linearly changed from 16 K to 26 K, large-scale divergence varies independently from zero to $6 \times 10^{-6}$ s$^{-1}$, and the entrainment ratio $\gamma = 0.5$. The model simulated relationship between mean surface wind and mean cloud fraction agrees well with both satellite observations shown in Figure 1 and ERA40 reanalysis results shown in Figure 2 in the southeast Pacific.

# 5. A stochastically perturbed model for surface wind probability distributions

## 5.1. Model descriptions

The model to describe the surface wind anomaly, boundary layer height, and marine cloud anomaly from mean states can be obtained from the deterministic model in Equations (22)-(25). Horizontal transport of eddies and fluctuations of unit area cloud radiative cooling are added as random perturbations in the original deterministic model.

$$\partial_t U' = a_u (\theta_{700} - T_s) \frac{h'}{\Delta \theta_0} + f V' + D_{z_i} U' - C_d \left( \overline{V_s} + V_s' \right) \frac{U'}{h_0} - \partial_x \left( \overline{u'u'} \right) - \partial_y \left( \overline{u'v'} \right), \quad (26)$$

$$\partial_t V' = a_v (\theta_{700} - T_s) \frac{h'}{\Delta \theta_0} - f U' + D_{z_i} V' - C_d \left( \overline{V_s} + V_s' \right) \frac{V'}{h_0} - \partial_x \left( \overline{u'v'} \right) - \partial_y \left( \overline{v'v'} \right), \quad (27)$$

$$\partial_t h' = \frac{\left( \gamma F^0_{crf} C'_f Z_T \right)}{\left( \overline{h} + h' \right) \left( \theta_{Z_T} - T_s \right)} - D_{z_i} h' + \frac{c_1 C_f F'_{crf}}{h}, \quad (28)$$

$$0.3 c_p \left( D_{z_i} h' (\theta_{700} - T_s) - \left( t_u U' + t_v V' \right) \right) + a_c V_s' \Delta q_0 \left[ 1 - \frac{\theta_{Z_T} - T_s}{\Delta \theta_{\max}} \right] = C'_f F^0_{crf}. \quad (29)$$

The surface pressure gradient is determined by a mixing layer depth perturbation and ocean surface SST.

### 5.1.1. Random fluctuation parameterization for surface wind moments

Horizontal turbulent fluctuations of surface zonal wind and meridional wind are neglected in the deterministic model for mean states. However, in small time scale and space scale variations, horizontal eddy transport become important and complicated, which can be parameterized as

$$\partial_x \left( \overline{u'u'} \right) - \partial_y \left( \overline{u'v'} \right) = V_s \left[ C_u \left( \partial_x u' + \partial_y v' \right) \right] = V_s' \left[ S_u \dot{W}_u \right], \quad (30)$$

$$\partial_x\left(\overline{u'v'}\right)-\partial_y\left(\overline{v'v'}\right)=V_s\left[C_v\left(\partial_x v'+\partial_y v'\right)\right]=V_s'\left[S_v\dot{W}_v\right] \quad (31)$$

The horizontal gradient of surface wind perturbation is affected by ocean surface waves and eddies of small scale and mesoscale. The total effects resemble a random process with fluctuation strength proportional to the surface wind speed. In Equations (30) and (31), $\dot{W}$ is a random number between -1 and 1, $S_u$ and $S_v$ are defined as strengths of momentum random force per unit wind speed for zonal wind and meridional wind respectively.

#### 5.1.2. Random fluctuation parameterization for boundary layer height

Cloud top radiative cooling and surface flux are affected not only by ocean surface and atmospheric mean properties, but are also strongly affected by random process due to water droplet and evaporation fluctuations. This study separates the unit area cloud top radiative cooling $F_{crf}^0$ into its mean part $\overline{F_{crf}^0}$ and random part $\left(F_{crf}^0\right)'$, and assuming other random process independent of marine cloud fractions, the boundary layer height equation becomes

$$\partial_t h=\frac{\left(\gamma F_{crf}^0 C_f' Z_T\right)}{\left(\overline{h}+h'\right)\left(\theta_{Z_T}-T_s\right)}-D_{zi}h+S_{crf}\dot{W}_h, \quad (32)$$

$$S_{crf}\dot{W}=\frac{c_1\overline{C_f}\left(F_{crf}^0\right)'}{h}. \quad (33)$$

In the Equations (32) and (33), $S_{crf}$ represents the strength of entrainment rate fluctuations due to variations of unit area cloud top radiative cooling. It is still a big challenge to accurately estimate the amplitude of entrainment random perturbations. However, one major finding in the 2001 EPIC field study [21] is that boundary layer height variation is surprising high, at around 100 ~ 300 m/3 hr in the southeast Pacific region during the MSC maximum season. Based on this observation, it is reasonable to assume that the boundary layer height random perturbation rate could have similar amplitudes as that due to large-scale divergence. For a simulation of the model, we use $b\overline{C_f}=6$ mm/s. In Section 5.2, random perturbation coefficients are allowed to change in order to study how they affect the surface wind standard deviation and skewness. In summary, the stochastic model for surface wind, boundary layer height and marine low clouds are obtained from Equations (26)-(33).

$$\partial_t U'=a_u\left(\theta_{700}-T_s\right)\frac{h'}{\Delta\theta_0}+fV'-C_d\frac{\left(\overline{V_s}U'+V_s'\overline{U}\right)}{h_0}+V_s'S_u\dot{W}_U, \quad (34)$$

$$\partial_t V'=a_v(\theta_{700}-T_s)\frac{h'}{\Delta\theta_0}-fU'-C_d\frac{\left(\overline{V_s}V'+V_s'\overline{V}\right)}{h_0}+V_s'S_v\dot{W}_v, \quad (35)$$

$$\partial_t h'=\frac{\left(\gamma F_{crf}^0 C_f' Z_T\right)}{\left(\overline{h}+h'\right)\left(\theta_{Z_T}-T_s\right)}-D_{zi}h'+S_{crf}\dot{W}_h, \quad (36)$$

$$C_f'=0.3c_p\left(D_{z_i}h'(\theta_{700}-T_s)-\left(t_u U'+t_v V'\right)\right)+a_c V_s'\Delta q_0\frac{\left[1-\frac{\theta_{Z_T}-T_s}{\Delta\theta_{\max}}\right]}{F_{crf}^0}. \quad (37)$$

In the following model simulations, surface wind speed $V_s$ is calculated using both the model simulated surface wind anomaly and QuikSCAT three-year averaged seasonal winds.

## 5.2. Stochastic methods

The method to obtain model solutions forced by random perturbations is as follows: For any given initial conditions, it is assumed that the time interval for external random forcing is much longer than the time needed for convective boundary layer wind to reach its equilibrium solution, which is typically between 20 minutes to 1 hour. Considering a given set of initial condition $(U_0(i), V_0(i), H_0(i))$ and a random perturbation $\Sigma\dot{W}(i)$, a set of stable state solutions could be obtained $(U_*(i), V_*(i), H_*(i))$ based on the Equations (34)-(37), and Euler forward time iterations until a variable satisfies $X(t)-X(t-1)\leqslant\varepsilon\Delta t$. For any given set of initial conditions $(U_0(m), V_0(m), H_0(m))$, the mean value, the standard deviation, and the skewness of surface wind are obtained $(\text{mean}(X), \text{std}(X), \text{skw}(X))$, $X\in(U, V, H)$ using the following procedure. Given a series of random perturbations $\dot{W}(i), i=1,2,\ldots,N$, a series of stable solutions could be obtained $(U_*(i), V_*(i), H_*(i))$, $i=1,2,\ldots,N$, and their statistical values calculated based on the following definitions:

$$\mathrm{MEAN}(X) = \frac{1}{N}\sum_{i=1}^{N} X(i), \tag{38}$$

$$\mathrm{STD}(X) = \sqrt{\frac{1}{N-1}\sum_{i=1}^{N}\left(X(i)-\overline{X}\right)^2}, \tag{39}$$

$$\mathrm{SKEW}(X) = \frac{\left(\frac{1}{N}\sum_{i=1}^{N}\left(X(i)-\overline{X}\right)^3\right)}{(\mathrm{STD}(X))^3}. \tag{40}$$

Here MEAN($X$) is the mean value of a given random variable $X(n)(n = 1, 2, ..., N)$; STD($X$) is called the standard deviation of $X$ which is a measure of the degree to which the values of $X$ deviate from the mean value; SKEW($X$) is the skewness of $X$, the normalized third-order moment, a measure of the lopsidedness of the PDFs.

## 5.3. Simulation results

As shown in the stochastic model of Equations (34)-(37), the departure of surface winds from their seasonal cycles is determined by surface pressure gradient perturbations, the Coriolis force, surface friction, and momentum random forces. The surface pressure gradient depends on ocean surface SST and the boundary layer height anomaly. The time derivation of the boundary layer height anomaly is controlled by the marine cloud fraction anomaly, large-scale divergence, and random entrainment fluctuations. Previous studies observed a positive relationship between the standard deviations of surface wind speed with strengths of random fluctuations and a negative relationship between the skewness and its mean value of surface wind due to surface friction in global scales [7, 9]. In subtropical marine clouds regions, both marine cloud top radiation cooling and surface friction affect the surface wind probability distribution. The following questions are still under dabate: What are the observed relationships among the mean surface wind speed, its higher order moments, and ocean surface SST in the subtropical MSC regions? How does ocean surface SST, large-scale divergence, cloud internal fluctuations, and eddy transport fluctuations affect these relationships?

### 5.3.1. The relationship between higher moments of SWS and mean SWS

Figure 5 is the model-simulated SWS standard deviation (upper panel) and the skewness (lower panel) as functions of mean non-seasonal SWS near the Peruvian region, which is consistent with observational results shown in Figure 3. In the simulation, the large scale divergence is set to $3 \times 10^{-6}$ s$^{-1}$, the entrainment ratio is set to 0.2, the strength of momentum random force is given as $S_u = S_v = 4.5 \times 10^{-5}$ s$^{-1}$, and the strength of entrainment fluctuation is given as $S_{crf} = 1 \times 10^{-3}$ m/s. SST is linearly changed from 16°C to 26°C. The surface wind standard deviation is primarily determined by the strength of momentum random forcing and the strength of cloud internal fluctuations. It is also influenced by large-scale divergence. Influences of various factors on standard deviations are discussed further in Section 5.2. Both QuikSCAT observed skewness displayed in Figure 3 and the model simulated surface wind skewness shown in Figure 5 have a nonlinear relationship with its mean value. In large wind regimes, the stronger the wind speed, the larger the surface friction becomes, and the greater tendency of SWS-PDF towards extremely small values. However, in small wind regimes, increasing mean value of SWS leads to stronger cloud top radiative cooling, and the resulting mixing layer deepening further enhances the strength of momentum fluctuations, pushing the SWS-PDF towards an extremely large value. Cloud top radiative cooling, boundary layer deepening, and SWS fluctuations are tightly coupled in determining the SWS-PDF, particularly for small wind conditions.

### 5.3.2. Influences of various factors on SWS-PDF

Figure 7 is the model simulated standard deviations of surface wind speed plotted against varying; (a) large scale divergence ($\times 10^{-6}$ s$^{-1}$), (b) entrainment ratio, (c) strength of momentum random force ($4.5 \times 10^{-5}$ s$^{-1}$), and (d) strength of entrainment fluctuations ($1 \times 10^{-3}$ m/s). The model-simulated relationships between standard deviation and its mean value of SWS are significantly different when large-scale divergence is different. The model-simulated standard deviation is linearly increased with mean SWS when large-scale divergence is small. However, it has two peak values with mean wind speed when large-scale divergence is large. The standard deviation also has two peak values when the entrainment fluctuation strength is small, and is linearly increased with mean surface wind speed when the entrainment fluctuation strength is large. Increasing the strength of momentum fluctuations and entrainment ratio will increase the value of standard deviations. The theoretical explanation of this is for a future research.

Figure 8 is the model simulated skewness of SWS plotted against mean SWS with varying; (a) large scale divergence ($\times 10^{-6}$ s$^{-1}$), (b) entrainment ratio, (c) strength of momentum random force ($4.5 \times 10^{-5}$ s$^{-1}$), and (d) strength of entrainment fluctuations ($1 \times 10^{-3}$ m/s). Skewness is increased with mean SWS in when the wind speed is smaller than a critical value due to the buoyancy effect; and decreased with mean SWS in large wind regimes.

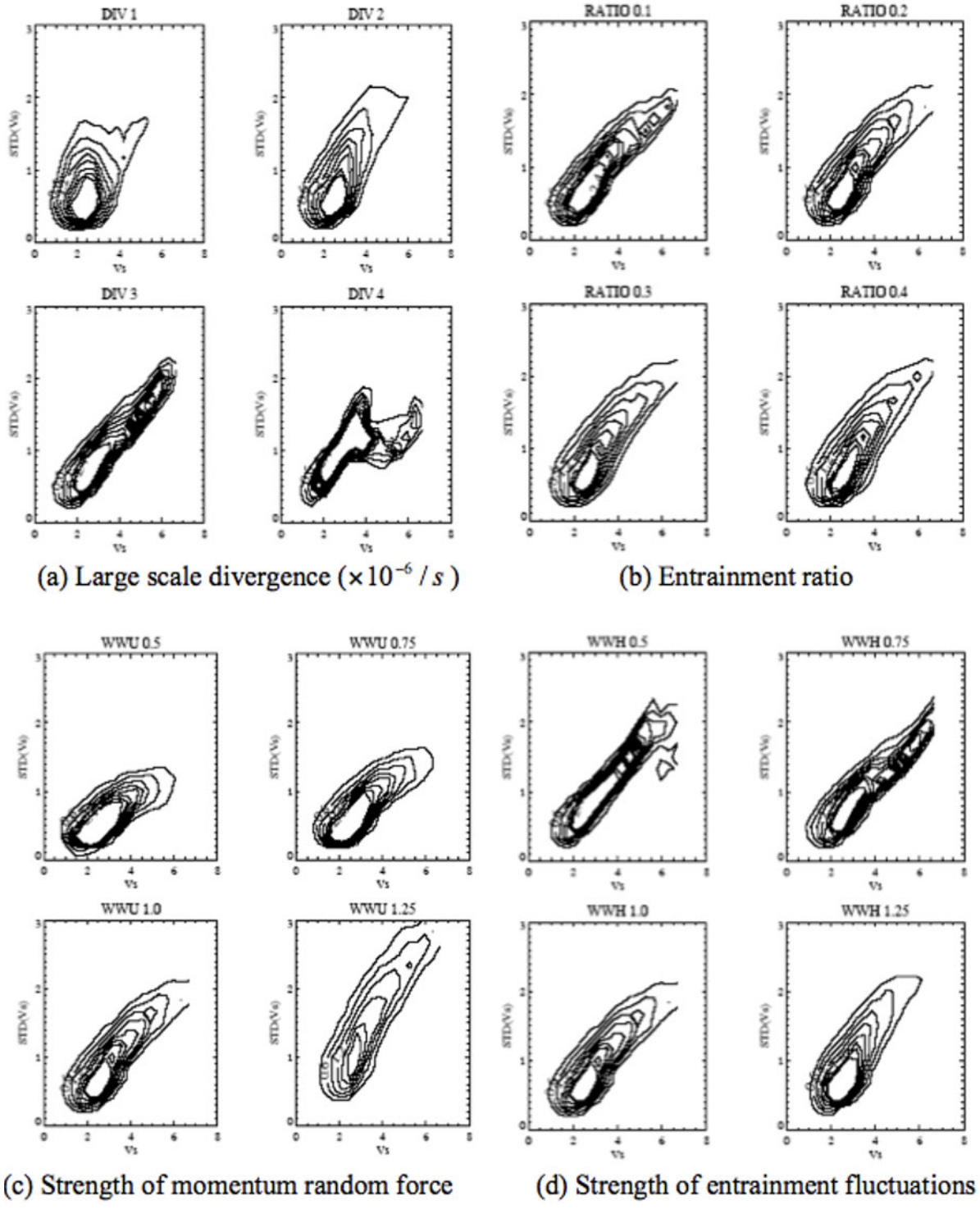


**Figure 7.** Model simulated standard deviations of surface wind speed plotted against surface wind speed with varying (a) large scale divergence ($\times 10^{-6}$ s$^{-1}$), (b) entrainment ratio, (c) strength of momentum random force ($4.5 \times 10^{-5}$ s$^{-1}$), and (d) strength of entrainment fluctuations ($1 \times 10^{-3}$ m/s).

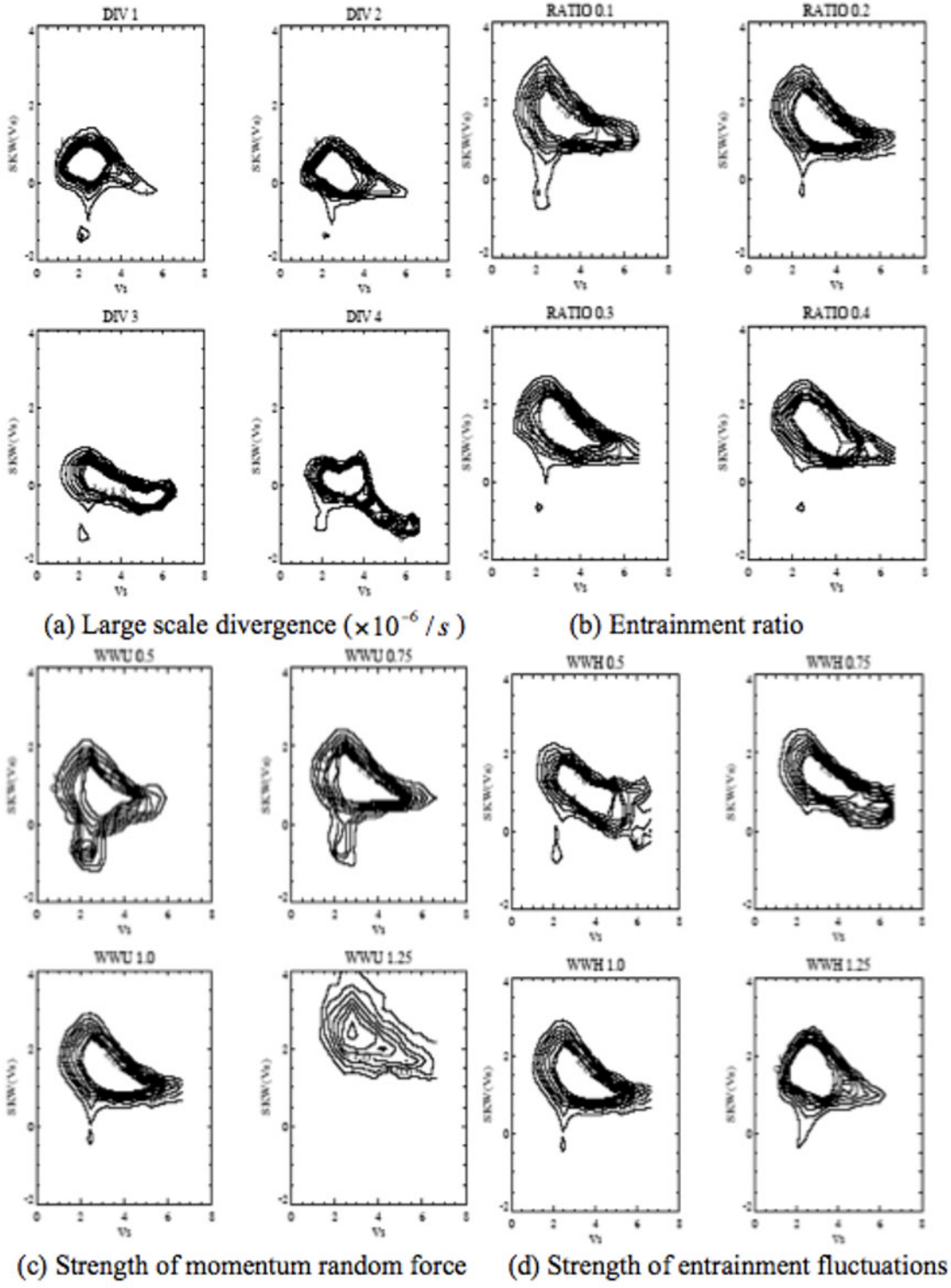


**Figure 8.** Model simulated skewness of surface wind speed plotted against surface wind speed with varying (a) large scale divergence ($\times 10^{-6}$ $s^{-1}$), (b) entrainment ratio, (c) strength of momentum random force ($4.5 \times 10^{-5}$ $s^{-1}$), and (d) strength of entrainment fluctuations ($1 \times 10^{-3}$ m/s).

The relationship between skewness and its mean value of SWS is greatly influenced by large-scale divergence, the strength of momentum fluctuations, and the strength of entrainment fluctuations. Increasing large-scale divergence or decreasing strengths of entrainment fluctuations both result in the shift of critical SWS value toward larger values. In other words, the tendency toward extremely large SWS is enhanced when large-scale divergence is strong and/or the strength of entrainment fluctuations due to unit of cloud top radiative cooling perturbation is small. Skewness values become larger in most SWS regimes when the strength of wind momentum fluctuations increases. Skewness decreases faster with mean SWS when the entrainment ratio is increased.

## 6. Conclusions

Probability distributions of surface wind speeds (SWS) near coastal regions have important applications in offshore wind power forecast and management, ocean surface flux parameterization and estimation, and extreme wind risk assessment. In this study, ocean surface wind speed probability distribution (PDF) is characterized based on three-year QuikSCAT and AIRS satellite observations in marine stratus and stratocumulus (MSC) regions of the southeast Pacific. Seasonal variation is removed from wind statistics. The second moment of SWS (standard deviation) is found to have a linear positive relationship with its mean value; while the third moment of SWS (skewness) is found to decrease with mean SWS in regimes of strong winds but increases with mean SWS in regimes of weak winds.

A simple 1D conceptual model is developed near the Peruvian region, which successfully reproduces the observed relationship between mean SWS and marine low cloud fraction and the relationship between higher moments of SWS and its mean value. The model based physical picture among ocean surface winds, ocean surface SST, and marine boundary clouds are supported by three-year QuikSCAT surface wind observations and fifteen-year ERA40 re-analysis data. Model sensitive tests suggest that large-scale divergence, and strengths of momentum and cloud fluctuations have significant effects on the ocean SWS-PDF in marine stratus and stratocumulus regions.

## Acknowledgements

The author thanks Dr. Robert E. Dickinson at the University of Texas, Austin, and Dr. Adam Hugh Monahan at the University of Victoria for insights, suggestions and help. This work was supported by NSF grant number ATM 0343485.

## References

[1] Jagger T., Sner J. B.E., X. Nu, A Dynamic probability model of hurricane winds in coastal counties of the United States, J. Appl. Meteorol., 40, 853-863, 2001

[2] McQueen D., S. Watson, Validation of wind speed prediction methods at offshore sites, Wind Energy, 2006, 9, 75-85

[3] Monahan A. H., A simple model for the skewness of global sea-surface winds, J. Atmos. Sci., 61, 2037-2049, 2004

[4] Petersen E.L., Mortensen N. G., Landberg L., Hojstrup J., Frank H. P., Wind power meteorology. Part I: Climate and turbulence, Wind Energy, 1998, 1, 25-45

[5] Isemer H., Hasse L., The scientific Beaufort equivalent scale: Effects on wind statistic and climatology and oceanography, B. Am. Meteorol. Soc., 1991, 79, 1855-1870

[6] Liu W. T., W. Tang, X. Xie, Wind power distribution over the ocean, Geophys. Res. Lett., 2008, 35, L13808

[7] Monahan A.H., Stochastic Dynamics of Sea Surface Winds. Proceedings, Workshop on Representation of Sub-Grid Processes Using Stochastic Dynamic Models (June 2005, Reading, UK), Shinfield Park, Reading, UK, 2006

[8] Nigam S., The Annual Warm to Cold Phase Transition in the Eastern Equatorial Pacific: Diagnosis of the Role of Stratus Cloud-Top Cooling, J. Climate, 1997, 10, 2447-2467

[9] Monahan A.H., The Probability Distribution of Sea Surface Wind Speeds. Part I: Theory and SeaWinds Observations, J. Climate, 2006, 19, 497-520

[10] Thompson K., Marsden R., Wright D., Estimation of low-frequency wind stress fluctuations over the open ocean, J. Phys. Oceanogr., 1983, 13, 1003-1011

[11] Wanninkhof R., Doney S. C., Takahashi T., McGillis W. R., The effect of using time-averaged winds on regional air-sea CO2 fluxes. In: Donelan M. A., Drennan W. M., Saltzman E. S., Wanninkhof R. (Eds.), Gas Transfer at Water Surfaces, American Geophysical Union, 2002, 351-356

[12] Lindzen R.S., S. Nigam, On the role of sea surface temperature gradients in forcing low-level winds and convergence in the Tropics, Journal of Amtospheric Science, 1987, 44, 2418-2436

[13] He Y., Representations of Boundary Layer Cloudiness and Surface Wind Probability Distributions in Sub-

tropical Marine Stratus and Stratocumulus Regions, PhD thesis, Georgia Institute of Technology, 2007
[14] Risien C. M., Chelton D. B., A global climatology of surface wind and wind stress fields from eight years of QuikSCAT scatterometer data, J. Phys. Oceangr., 2008, 38, 2379-2412
[15] Sampe T., Xie S.P.,Mapping high sea winds from space: a global climatology, B. Am. Meteorol. Soc., 2007, 88, 1965-1978
[16] Rossow W. B., Schiffer R. A., ISCCP cloud data products, B. Am. Meteorol. Soc., 1991, 72, 2-20
[17] Uppala S.M., Kallberg P.W., Simmons A.J., Andrae U., Da Costa Bechtold V., Fiorino M. et al., The ERA-40 re-anaysis, Q. J. Roy. Meteor. Soc., 2005, 131, 2961-3012
[18] Larson K., Hartmann D. L., The role of clouds, water vapor, circulation, and boundary layer structure in the sensitivity of the tropical climate, J. Climate, 1999, 13, 2359-2374
[19] Wood R., Hartmann D.L., Spatial variability of liquid water path in marine boundary layer clouds. Part I: the importance of mesoscale cellular convection, J. Climate, 2006, 19, 1748-1764
[20] Lilly D. K., Models of Cloud-Topped Mixed Layers under a Strong Inversion, Q. J. Roy. Meteor. Soc., 1968, 94, 292-309
[21] Bretherton C.S., Uttal T., Fairall C.W., Yuter S.E., Weller R.A., Baumgardner D. et al., The EPIC 2001 Stratocumulus Study, B. Am. Meteorol. Soc., 2004, 85, 967-977
[22] Rozendaal M.A., Rossow W.B., Characterizing some of the influences of the general circulation on subtropical marine boundary layer clouds, J. Atmos. Sci., 2003, 60, 711-728
[23] Stevens B., Zhang Y., Ghil M., Stochastic effects in the representation of stratocumulus-topped mixed layers, ECMWF Workshop on Representation of Sub-grid Processes Using Stochastic-Dynamic Models, (June 2005, Reading, UK), Shinfield Park, Reading, UK, 2006
[24] Wood R., Bretherton C., On the relationship between stratiform low cloud cover and lower tropospheric stability, J. Climate, 2006, 19, 6425-6432
[25] Xu H.M., Xie S.P., Wang Y.Q., Subseasonal variability of the southeast Pacific stratus cloud deck, J. Climate, 2005, 18, 131-142